A Facile Preparation of Palladium Nanoclusters Supported on Hydroxypropyl-β-Cyclodextrin Modified Fullerene [60] for Formic Acid Oxidation

Zhengyu Bai, Lu Niu, Shujun Chao, Huiying Yan, Qian Cui, Lin Yang[*], Jinli Qiao[*], Kai Jiang

[1] School of Chemistry and Chemical Engineering, Henan Normal University; Key Laboratory of Green Chemical Media and Reactions, Ministry of Education, Xinxiang 453007, P. R. China
[2] College of Environmental Science and Engineering, Donghua University, Shanghai 201620, P. R.China.
[*] E-mail: yanglin1819@163.com; qiaojl@dhu.edu.cn

The use of fullerene [60] (C_{60}) as carbon support material assists the dispersion of catalysts and provides new ways to develop advanced electrocatalyst materials as a result of its distorted structure. However, C_{60} cannot be readily dispersed in water because of its hydrophobic properties. In this paper hydroxypropyl-β-Cyclodextrin (HP-β-CD) modified C_{60} (abbreviated as HP-β-CD-C_{60}) is introduced and palladium nanoclusters, composed of nanoparticles supported on HP-β-CD-C_{60} (Pd/HP-β-CD-C_{60}) are successfully prepared. The results of transmission electron microscopy measurements show that the novel as-prepared nanoclusters Pd catalyst, dispersed on HP-β-CD modified C_{60}, is composed of Pd nanoparticles, in which the average size of the Pd nanoparticles is 2.5 nm. Cyclic voltammograms for the oxidation of pre-adsorbed CO demonstrate that the Pd/HP-β-CD-C_{60} nanocomposites, with an electrochemical surface area of 41.6 m^2 g^{-1}, show excellent electrocatalytic activity. From the cyclic voltammetry and chronoamperometry results for formic acid oxidation, the Pd/HP-β-CD-C_{60} modified electrode reveals a significantly high electrocatalytic activity, much more negative onset potentials and better stability than electrodes modified by other electrocatalysts, which indicates that it is a better potential candidate for application in a direct formic acid fuel cell (DFAFC).

1. INTRODUCTION

In order to satisfy mankind's ever-increasing energy needs and to manage serious environmental issues, it is essential to consider alternative energy sources to replace the currently

dominant fossil fuels, such as petroleum and natural gas. Fuel cells have attracted considerable attention as green power sources for vehicles, portable electronics and space navigation, due to their high efficiency and negligible pollution [1-2]. Of the various types of fuel cell, the direct formic acid fuel cell (DFAFC), which is based on liquid fuels, has attracted significant attention as a power source for portable electronic devices owing to its high energy density, low operating temperature and because it is non-toxic, which is not true for gaseous fuels [3-5]. However, several problems including inadequate activity and the high cost of anode catalysts, need to be resolved before DFAFCs can be commercialized [6]. To solve these problems, tremendous efforts have been made to prepare well-defined nanostructured catalysts with promising catalytic performance. On the one hand, less expensive and more abundant non-platinum catalysts with acceptable performance have been widely studied [7-9]. For instance, Pd and Pd derivatized-catalysts, which have good electrocatalytic activity and excellent anti-CO toxic ability, have recently been used in DFAFCs [10-11]. On the other hand, the choice of a suitable support is another key factor affecting the electrocatalytic performance of the catalysts, because it can affect the size and dispersion of the metal nanoparticles [12-13].

Considerable effort in this field has been devoted to explore new supports for catalysts, intended to achieve high dispersion, utilization, activity and stability [14]. Various carbon materials, such as carbon black and carbon nanotubes, have been extensively investigated as possible electrocatalyst supports in fuel cells. Some novel carbon materials have also been proposed, such as graphite nanofibers (GNFs), graphitic carbon nanocoils (GCNC), graphene and fullerene [15-18]. Among them, the use of fullerene [60] (C_{60}) as a support material introduces a new strategy to develop advanced electrocatalyst materials as a result of its distorted structure. In addition, this distortion may provide strong adsorption possibilities for metal nanoparticles and so produce novel catalytic properties [19]. Due to the strong attachment to metals and its chemical inertness, C_{60} moieties have also been used as seeds for the growth of highly dispersed Pt nanoparticles, which exhibit remarkable methanol oxidation activity [20]. Generally, C_{60} can be readily dispersed in organic solvents but not water, due to its hydrophobic properties. To tackle this problem, we have considered the use of hydroxypropyl-β-cyclodextrin (HP-β-CD), one of the most commonly used agents in the synthesis of metallic and semiconductor nanoparticles because it can act as a surfactant and coordination agent, simultaneously. Many inorganic nanoparticles (such as CuS, CdS), with small particle size, have been synthesized in the presence of HP-β-CD [21-22]. What is novel is that, with the help of HP-β-CD, C_{60} can be well dispersed in water [23], to afford a harmless, nonpoisonous, and environmentally friendly reaction system.

In this work, a novel synthetic route for the preparation of Pd nanoparticles with small particle size supported on HP-β-CD modified C_{60} (abbreviated as HP-β-CD-C_{60}) in aqueous solution is reported. By simultaneously applying HP-β-CD as the surfactant and coordination agent, Pd nanoclusters with a particle size below 3 nm were successfully prepared using a potassium borohydride reduction process. Due to the enhanced dispersity and compositional uniformity of Pd nanoparticles with HP-β-CD, the as-prepared Pd/HP-β-CD-C_{60} catalyst showed large ECSA and therefore excellent electrocatalytic activity.

2. EXPERIMENTAL

2.1. Materials

Potassium borohydride (KBH$_4$), hydroxypropyl-β-cyclodextrin, ethanol, formic acid, sulfuric acid, and nitric acid were purchased from China National Pharmaceutical Group Corp., PdCl$_2$ was obtained from Alfa Aesar, C$_{60}$ was purchased from Puyang Yongxin Fullerene Technology Co., Ltd., and Vulcan XC-72 carbon powder from Cabot Company. All chemical reagents used in this experiment were of analytical grade and were used as received without further purification. Double distilled water (DD water) was used in all of the experiments.

2.2. Preparation of Pd/HP-β-CD-C$_{60}$ catalyst

In brief, 40 mg C$_{60}$ were dispersed in 75 mL DD water containing 500 mg HP-β-CD by ultrasonication for 30 min and kept stirring for 30 min. Subsequently, 10 mL PdCl$_2$ (0.02 M) aqueous solution was slowly added into the system under stirring and the pH was adjusted to 10 using 0.5 M NaOH solution. Then the mixture was stored at room temperature overnight. A freshly prepared KBH$_4$ solution (60 mg in 60 mL DD water) was added dropwise into the above mixture under moderate stirring for 2 hr, and then the stirring was continued for another 2 hr to make sure the completely reduction of Pd^{2+}. The whole process was operated at room temperature. Finally, the product was collected by filtration and washed several times, then dried at 40°C under vacuum for 12 hr, and Pd/HP-β-CD-C$_{60}$ electrocatalyst was obtained.

### 2.3. Catalyst physical and electrochemical characterizations

The as-prepared nanoparticles were dispersed into ethanol by ultrasonication for 5 min. And then, a drop of the suspension was then deposited on a lacey carbon grid and dried in air for TEM observations. The morphology of the as-prepared catalyst was measured by JEOL-100CX high resolution transmission electron microscopy (HRTEM) operated at 200 kV and JSM-6701F scanning electron microscopy (SEM). X-ray powder diffraction (XRD) measurements were performed on a Bruker D&Advance X-ray powder diffractometer with graphite monochromatized Cu/KR (γ) 0.15406 nm). The thermogravimetric analysis (TGA) was performed on an NETZSCH STA 449C instrument under the protection of N$_2$ at a heating rate of 10 deg/min from 30 to 700 °C.

Cyclic voltammetry measurements were carried out in a three-electrode cell by using Solartron 1287 electrochemical test system (Solartron Analytical, England). A glassy carbon (GC) disk (3 mm o.d.) coated with catalyst was used as the working electrode, a platinum foil (1 cm^2) as the counter-electrode, and an Ag/AgCl electrode as the reference. For electrochemical measurements, a certain amount of Vulcan XC-72 was introduced into the system in order to improve the electroconductivity of the support. Briefly, 3 mg catalyst was suspended in 0.3 mL of isopropanol/Nafion solution (5 wt.%) to prepare the catalyst ink. Then 15 μL of ink was transferred with an injector to a clean GC disk electrode.

Electrochemical CO stripping voltammograms were obtained by oxidizing preadsorbed CO (COad) in 0.5 M H_2SO_4 at a scan rate of 20 mV s^{-1}. CO was purged through 0.5 M H_2SO_4 for 30 min to allow complete adsorption of CO onto the catalyst. The working electrode was stayed at 0.1 V (*vs.* Ag/AgCl), and excess CO in the electrolyte was removed by purging with high-purity N_2 for 30 min. The amount of COad was evaluated by integrating the COad stripping peak and correcting for the capacitance of the electric double-layer. The activity evaluation of catalysts toward formic acid oxidation was carried out in 0.5 M H_2SO_4 electrolyte containing 1 M HCOOH. The cyclic voltammetry were recorded by a linear potential scan at a sweep rate of 50 mV·s^{-1}, and chronoamperometry tests were carried out at 0.1 V for 6000 s. High-purity nitrogen was purged for 15 min before the test was performed, the potential range was form -0.2 to 0.8 V. All electrochemical experiments were performed at 25 ± 1 °C.

3. RESULTS AND DISCUSSION

We have described the preparation of Pd nanoclusters supported on HP-β-CD-C_{60} using a facile process at room temperature. For the synthesis of Pd/HP-β-CD-C_{60} hybrid nanoparticles, a two-step strategy was employed, involving the generation of HP-β-CD-C_{60} composites followed by the preparation of Pd nanoparitcles. A schematic route for preparation of the Pd nanocluster catalysts is presented in Fig. 1.
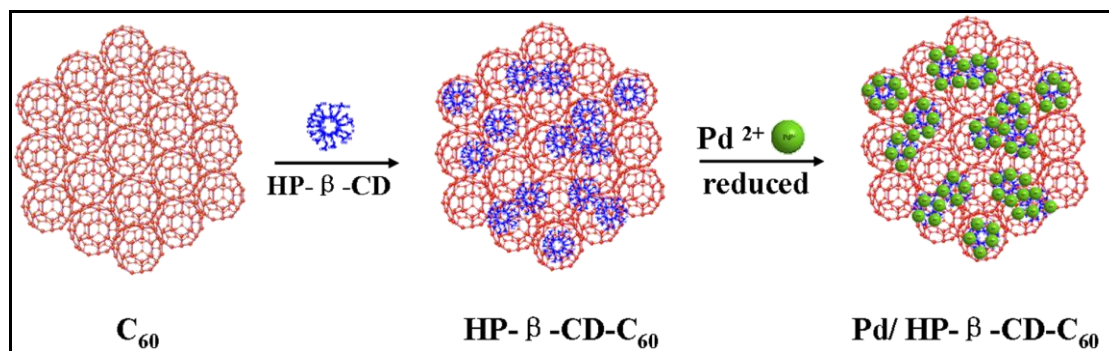
Figure 1. Schematic illustration of the formation of Pd/HP-β-CD-C_{60}.

Firstly, C_{60} can be evenly dispersed in water with the help of HP-β-CD, at which time an adsorption layer is formed on the surface of C_{60} by Van der Waals forces. Subsequently, Pd^{2+} ion is mixed with the HP-β-CD-C_{60} composites, so that the HP-β-CD is covered with Pd^{2+} through the coordination between the Pd^{2+} and the hydroxyl (-OH) on the surface of the HP-β-CD. Finally, the Pd^{2+} ion is reduced *in situ* to Pd nanoparticles with KBH_4 as the reducing agent, forming Pd nanoclusters in the presence of HP-β-CD. Consequently, HP-β-CD acts simultaneously as the surfactant and coordination agent. The stabilizing effect of the HP-β-CD may be attributed to the presence of bifunctional groups, which can act as an interlinker between the surface of the C_{60} and the

nanoparticles. On the one hand, the inner cavity of the HP-β-CD may interact with the surface of the C_{60} as a result of its hydrophobic features. On the other hand, the -OH groups on the external cavity may adsorb Pd^{2+} ions *via* electrostatic interactions, followed by the *in situ* formation of the corresponding nanoparticles on the C_{60}.
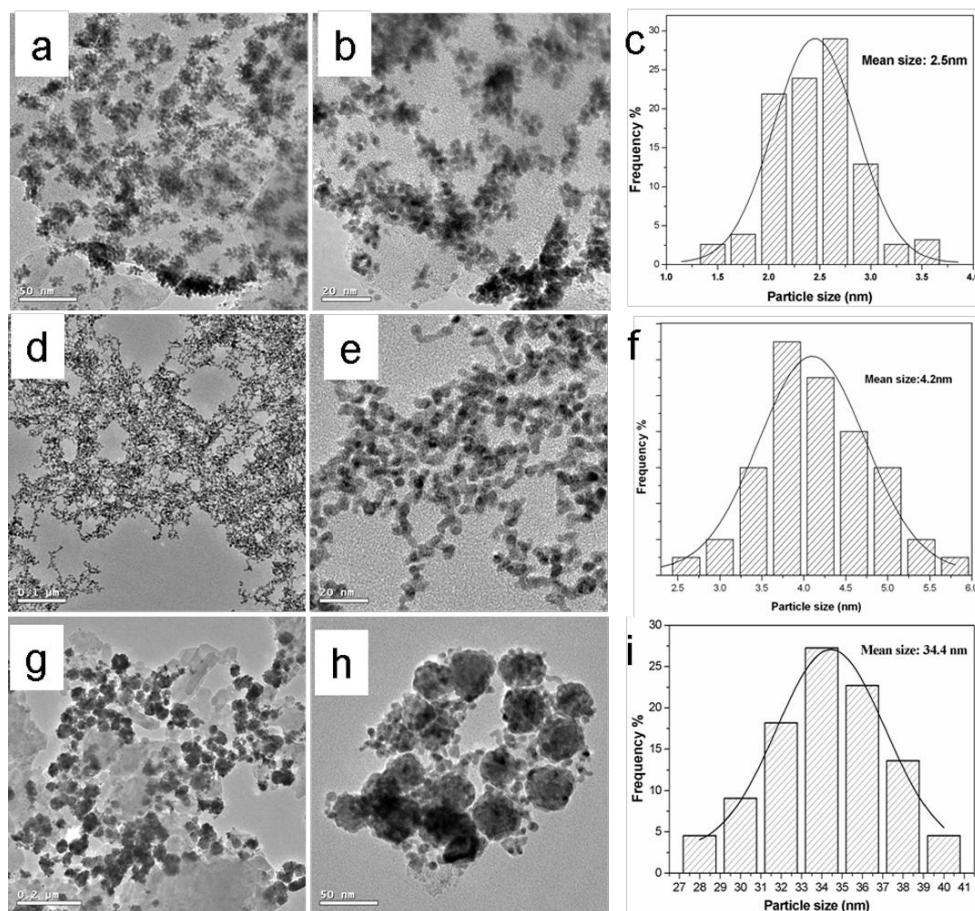
Figure 2. TEM images with different magnification and corresponding size distribution of synthesized (a-c) Pd/HP-β-CD-C_{60}, (d-f) Pd/HP-β-CD and (g-i) Pd/C_{60}.

The TEM images demonstrate that the Pd nanoclusters are composed of nanoparticles with much more uniform size and distribution than could be obtained using HP-β-CD-C_{60} as the composite support. The TEM images and the size distribution histrogram of the Pd/HP-β-CD-C_{60} catalyst are shown in Fig. 2(a-c). It can be seen that the Pd nanoclusters, composed of nanoparticles with a smaller particle size, are well-dispersed on the surface of the HP-β-CD-C_{60} composites (Fig. 2a). The diameters of the nanoparticles, as seen from the magnified TEM image (Fig. 2b), range from 1.3 to 3.8 nm and the mean size, calculated by the log-normal distribution, is 2.5 nm (Fig. 2c). To investigate the influence of HP-β-CD and C_{60} on the formation of the Pd nanoclusters, two sets of control experiments were carried out. Control A was carried out under the same conditions described as the typical experiment, apart from the absence of C_{60}. Control B was carried out by using C_{60} as support under the same conditions except for the absence of HP-β-CD. Fig. 2(d-f) and Fig. 2(g-i) show TEM images and

the size distribution histogram of the Pd/HP-β-CD and Pd/C$_{60}$, respectively. As can be seen in Fig. 2(d-f), Pd nanoparticles formed in control A are well-dispersed, with a relatively narrow particle size distribution of about 4.2 nm in diameter. On the other hand, much larger Pd nanoparticles, about 34 nm, are formed together with serious agglomeration, in control B (Fig. 2(g-i)), and the aggregates contain nanoparticles with a diameter of about 7 nm (Fig. 2h). This suggests that the HP-β-CD plays a key role in controlling and regulating the shape and size of the Pd nanoparticles. During the reaction process, immobilization of HP-β-CD on the surface of C$_{60}$ produces a uniform distribution of hydroxyl groups, which can serve as functional groups for the self-assembly of Pd precursors on the surface of C$_{60}$. In addition, the presence of C$_{60}$ may also be a useful way to increase the Pd metal loading through the adsorption of Pd particles on to the C$_{60}$. This can be confirmed by the elemental mapping measurements and FT-IR spectroscopy. Therefore, Pd nanoclusters composed of nanoparticles with a much more uniform size and distribution are formed. These can enhance the electrocatalytic activity and stability for formic acid oxidation.
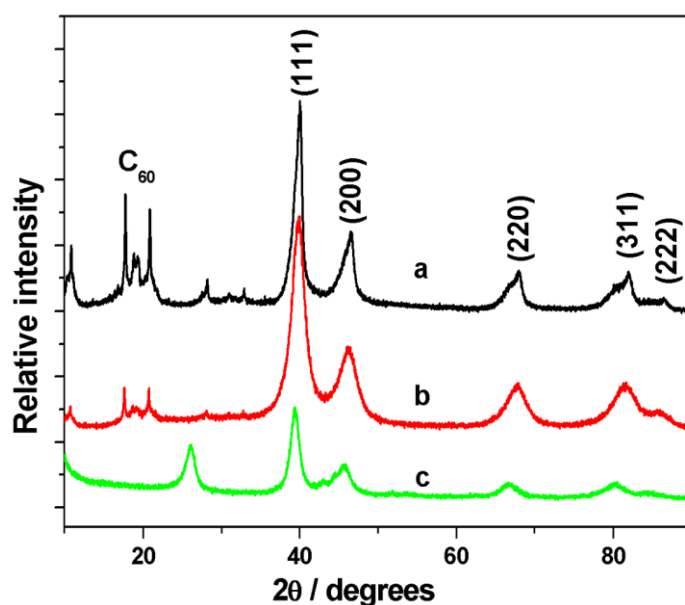

**Figure 3.** X-ray diffraction patterns of synthesized (a) Pd/C$_{60}$, (b) Pd/HP-β-CD-C$_{60}$ and (c) Pd/HP-β-CD.

Fig. 3 shows the XRD patterns of the as-prepared (a) Pd/C$_{60}$, (b) Pd/HP-β-CD-C$_{60}$ and (c) Pd/HP-β-CD. The five peaks, at 39.8°, 46.3°, 67.6°, 81.9° and 86.1°, are characteristics of face-centered-cubic (fcc) crystalline Pd, and correspond to the (111), (200), (220), (311) and (222) reflections, respectively [24]. There is also the characteristic peak of the C$_{60}$ support at around 20°. Clearly, HP-β-CD and C$_{60}$ have no significant influence on the crystalline form of the Pd nanoparticles. In addition, the full width at half maximum (FWHM) of the diffraction peaks of the Pd/HP-β-CD-C$_{60}$ are wider than those of the others, indicating the smaller particle size of the Pd nanoparticles supported on the HP-β-CD-C$_{60}$. This is in agreement with the results of the HRTEM and size distribution analysis.

In order to investigate whether the HP-β-CD is located on the surface of C_{60} or not, an elemental mapping measurement was performed. A study of the SEM image and TGA curves indicate that the HP-β-CD is successfully adsorbed on to the surface of the C_{60} crystal. Fig. 4 shows the SEM image and corresponding elemental mapping of the HP-β-CD-modified C_{60} composites. It can be seen clearly that C (Fig. 4b) and O (Fig. 4c) are well-dispersed on the surface of HP-β-CD-C_{60}, indicating the expected spatial distribution of HP-β-CD. The results show HP-β-CD exists on the surface of C_{60} crystals.
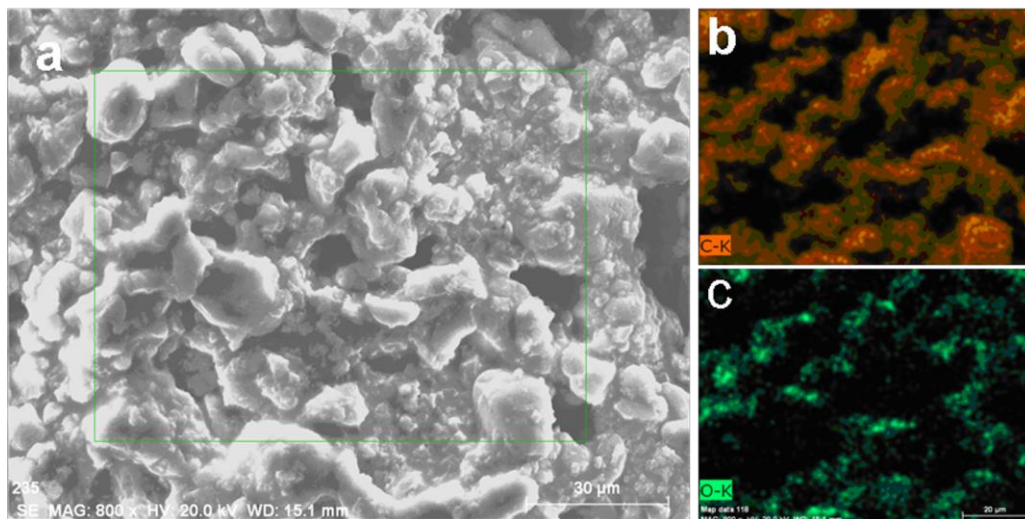
**Figure 4.** SEM image of (a) HP-β-CD-C_{60} and corresponding elemental mapping of (b) C elemental, (c) O elemental.
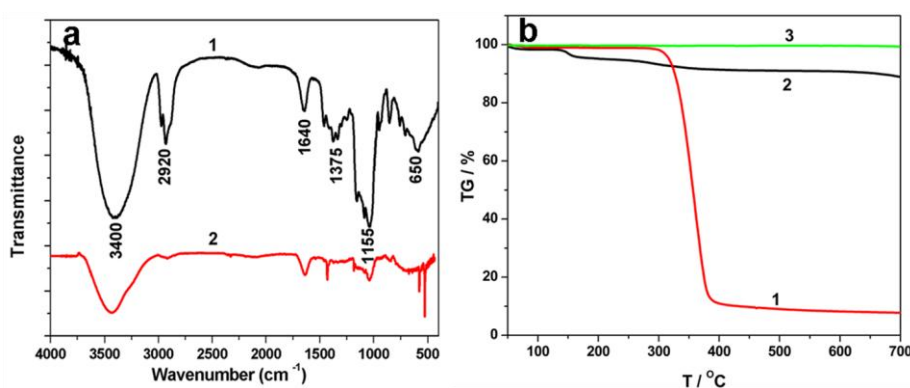
Figure 5. (a) FT-IR spectroscopy for HP-β-CD (curve 1) and HP-β-CD-C_{60} (curve 2), (b) TGA curves for HP-β-CD (curve 1), HP-β-CD-C_{60} composite (curve 2) and C_{60} (curve3)

To further study the effect of HP-β-CD on the C_{60} nanocrystals, FT-IR spectroscopy and TGA curves of the composites were investigated. Fig. 5a compares the FT-IR spectra of HP-β-CD (curve 1) and HP-β-CD-C_{60} composites (curve 2). In the IR spectrum of HP-β-CD, the peak located at about 3400 cm^{-1} is assigned to the stretching vibration of O-H, 2920 cm^{-1} to the stretching vibration of C-H, 1640 cm^{-1} to the flexural vibration in the plane of O-H, 1375 cm^{-1} to the symmetrical flexural vibration of the methyl group, 1155 cm^{-1} to the stretching vibration of C-O and 650 cm^{-1} to the out-of-plane

flexural vibration [25]. In the case of the HP-β-CD-C_{60} composites, all the peaks of HP-β-CD can be observed but, in addition, the C_{60} is characterized by the peaks at 526, 575, 1181 and 1428 cm^{-1}. From the IR data, it can be seen that the HP-β-CD-C_{60} composite has been successfully prepared. The TGA curves shown in Fig. 5b compare the thermal-decomposition curves of the pure HP-β-CD (curve 1), HP-β-CD-C_{60} composite (curve 2) and C_{60} (curve 3).
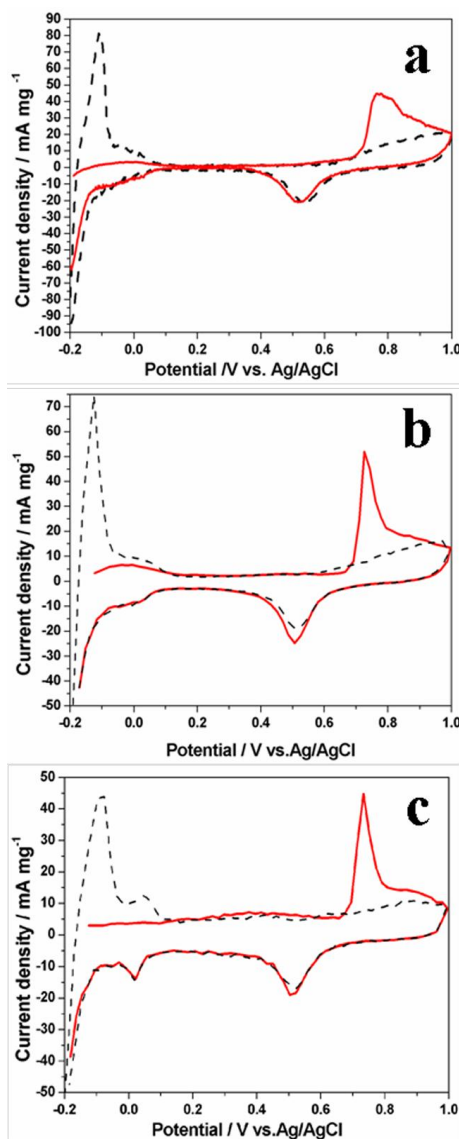
Figure 6. Cyclic voltammograms for the oxidation of pre-adsorbed CO(a) Pd/HP-β-CD-C_{60}, (b) Pd/HP-β-CD and (c) Pd/C_{60} in 0.5 M H_2SO_4. The solid curves were CVs for these electrodes without COad. The scan rate is 20 mV s^{-1}.

From curve 1, the TGA curve of HP-β-CD shows an obvious weight loss, from 300 to 400 °C, corresponding to the degradation of HP-β-CD. It is evident that HP-β-CD can be decomposed completely at 400 °C. Compared to HP-β-CD, the TGA curve of the HP-β-CD-C_{60} composite support shows a two-step weight loss. The first step (130-160 °C) can be attributed to a dehydration process

that corresponds to a loss of about 4.5 water molecules per HP-β-CD molecule. Similar results have been reported by Garnero et al [26]. The second step corresponds to the decomposition of HP-β-CD, and the content of HP-β-CD is about 5%. As observed in curve 3, there is no obvious weight loss in the heating process, indicating that C_{60} has good thermal stability. From Fig. 5b, the content of HP-β-CD in the HP-β-CD-C_{60} composite is about 5%. Overall, the results indicate that the HP-β-CD-C_{60} composite has been successfully prepared and HP-β-CD exists on the surface of the C_{60} crystal.

The electrochemical behaviors of the different catalysts were recorded using cyclic voltammetry (CV) measurements performed in 0.5 M H_2SO_4 electrolyte at a scan rate of 20 mV s^{-1}. Fig. 6 shows the CV curves obtained with CO adsorbed on to the catalysts (dashed curves) and without CO adsorbed (solid curves), of the as-prepared (a) Pd/HP-β-CD-C_{60}, (b) Pd/HP-β-CD and (c) Pd/C_{60}, respectively. It can be seen that the hydrogen adsorption peak on the Pd/HP-β-CD-C_{60} electrode is much larger than that on the Pd/HP-β-CD and Pd/C_{60} electrode, indicating the superior electrocatalytic activity of the Pd/HP-β-CD-C_{60} catalyst. The corresponding ECSA of the catalyst was obtained from Eq. (1) [27-28]:

$$ECSA = \frac{Q}{G \times 420} \quad (1)$$

where Q is the charge of the CO desorption-electrooxidation in microcoulomb (μC), G represents the total amount of Pd (μg) on the electrode, and 420 is the charge required to oxidize a monolayer of CO on the catalyst in μC cm^{-2}. The calculated ECSA values are 41.6, 37.9, and 24.6 m^2 g^{-1} for the as-prepared Pd/HP-β-CD-C_{60}, Pd/HP-β-CD and Pd/C_{60}, respectively. Clearly, the ECSA values for the Pd/HP-β-CD-C_{60} catalyst is much larger than the others, most likely due to the smaller size and better dispersion of the Pd nanoparticles on C_{60}, achieved with the aid of HP-β-CD. In theory, the larger the ECSA of a catalyst is, the higher electrocatalytic activity it will have. Hence, it also demonstrates that the Pd nanoparticles deposited on the surface of C_{60} are electrochemically more accessible, which is very important for electrocatalyst applications in fuel cells.
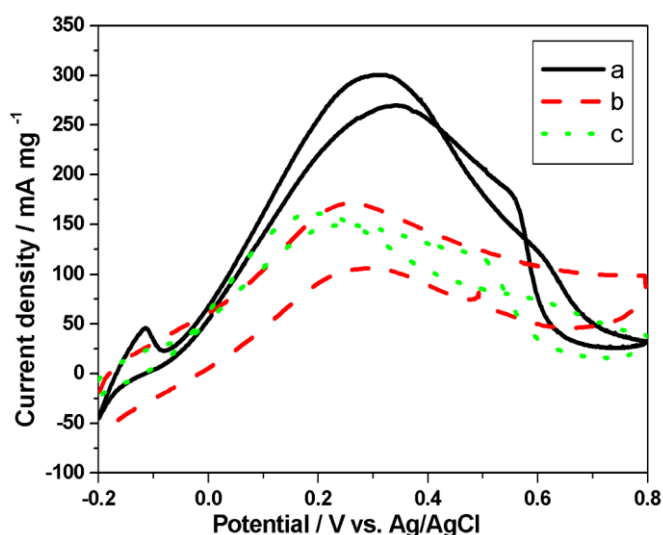
Figure 7. Cyclic voltammograms of synthesized (a) Pd/HP-β-CD-C_{60}, (b) Pd/HP-β-CD and (c) Pd/C_{60}, electrolyte: 0.5 M H_2SO_4 + 1 M HCOOH aqueous solution, sweep rate 50 mV s^{-1}, at 25°C

The electrocatalytic activities for formic acid oxidation using the as-prepared electrocatalysts were analyzed by CV measurement in 0.5 M H_2SO_4 containing 1 M HCOOH aqueous solution under half-cell conditions at a scan rate of 50 mV s^{-1}. Fig. 7 compares the CV curves of the as-prepared (a) Pd/HP-β-CD-C_{60}, (b) Pd/HP-β-CD, and (c) Pd/C_{60}. As can be seen in Fig. 7, the two main oxidation peaks of the catalysts are located at about 0.3 V in both the positive and negative scan direction, and the corresponding peak current density of Pd/HP-β-CD-C_{60} is about 300 mA mg^{-1}, much higher than those of the others. This demonstrates that the Pd/HP-β-CD-C_{60} modified electrode shows extraordinarily high electrocatalytic activity relative to the electrode modified by other electrocatalysts. From these results, we propose that the much higher electrocatalytic activity of Pd nanoparticles relies on the cooperation of Pd/HP-β-CD and C_{60}. Here, Pd/HP-β-CD is likely to control the size of the Pd nanoparticles through the coordination interaction between the -OH groups and Pd^{2+}, then C_{60} may enhance the metal loading through the adsorption of metal particles on to the C_{60}. In comparing the relative activity of these electrocatalysts, two parameters for fuel oxidation are of particular importance, the current density (which reflects the kinetic aspects) and the onset potential (which reflects the thermodynamic aspects). From Fig. 7, it can be clearly seen that the onset potentials for the formic acid electrooxidation on Pd/HP-β-CD-C_{60} catalyst is much more negative than those of the others. The lower onset potential and higher peak current density indicate that Pd/HP-β-CD-C_{60} has better electrocatalytic activity for the oxidation of formic acid.
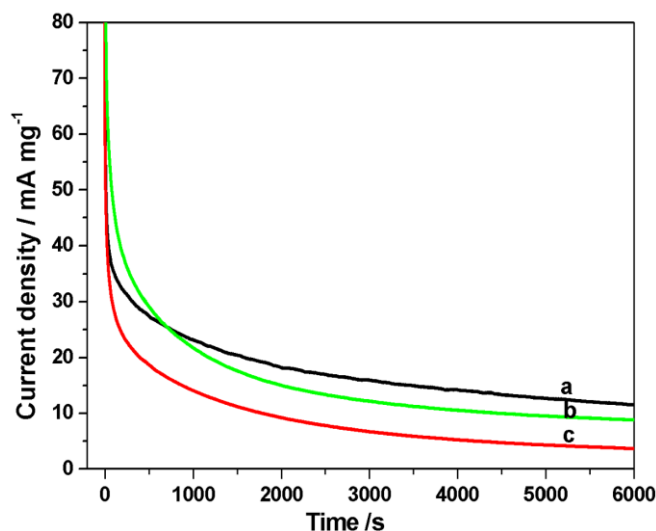
Figure 8. Chronoamperometry lines of as-prepared (a) Pd/HP-β-CD-C_{60}, (b) Pd/HP-β-CD and (c) Pd/C_{60}, electrolyte: 0.5 M H_2SO_4 + 1 M HCOOH aqueous solution at a potential of 0.1 V, at 25°C.

In order to compare the electrochemical stability of the as-prepared catalysts for formic acid oxidation, chronoamperometry tests were carried out in 0.5 M H_2SO_4 containing 1 M HCOOH aqueous solution at 0.1 V for 6000 s. Fig. 8 shows the chronoamperometric curves for Pd/HP-β-CD-C_{60}, Pd/HP-β-CD and Pd/C_{60}. As observed, curve b and curve c drop quickly at the beginning but a slower decrease is observed in curve a. In addition, the current density of the Pd/HP-β-CD-C_{60}, Pd/HP-

β-CD and Pd/C_{60} catalysts at 6000 s is 11.8, 8.8 and 3.6 mA mg^{-1}, respectively. It is clear that the Pd/HP-β-CD-C_{60} catalyst shows much higher anodic currents but much slower current degradation, demonstrating better activity and stability than that of the Pd/C_{60} catalyst under the same conditions. This makes Pd/HP-β-CD-C_{60} a very promising alternative as an anode catalyst for DFAFCs.

4. CONCLUSION

The Pd catalyst, consisting of nanoclusters supported on HP-β-CD-C_{60}, has been prepared using a facile chemical reduction method. The HP-β-CD-C_{60} composite can control the size and dispersivity of the Pd nanoparticles. Due to the high dispersivity and uniformity of the as-prepared Pd nanoparticles (2.5 nm), the Pd/HP-β-CD-C_{60} nanocomposites, with an electrochemical surface area of 41.6 m^2 g^{-1}, show extraordinarily high electrocatalytic activity for the oxidation of formic acid. The results demonstrate that Pd/HP-β-CD-C_{60} is a better potential candidate for application in DFAFCs.

References

1. S. S. Dihrab, K. Sopian, M. A. Alghoul, M. Y. Sulaiman, *Renew. & Sust. Energ. Rev*. 13 (2009) 1663-1668.
2. R. Bashyam, P. Zelenay, *Nature*, 443 (2006) 63-66.
3. C.Rice, S.Ha, R. I.Masel, P.Waszczuk, A.Wieckowski, T.Barnard, *J. Power Sources*. 111(2002) 83-89.
4. C.Rice, S.Ha, R. I.Masel, A.Wieckowski, *J. Power Sources*. 115(2003) 229-235.
5. S.Zhang, Y.Y.Shao, G.P. Yin, Y.H. Lin, *Angew. Chem. Int. Ed*. 49 (2010) 2211-2214.
6. R.F. Wang, H. Li, H.Q. Feng, H. Wang, Z.Q. Lei, *J. Power Sources* 195 (2010) 1099-1102.
7. E. Casado-Rivera, D.J. Volpe, L. Alden, C. Lind, C. Downie, T. Vazquez-Alvarez, A.C.D Angelo, F.J. DiSalvo, H.D. Abruna, *J. Am. Chem. Soc*. 126(2004) 4043−4049.
8. R.N. Bonifácio, A.O. Neto, M. Linardi, *Int. J. Electrochem. Sci*., 8 (2013) 159-167
9. Y.J. Kang, L. Qi, M. Li, R.E. Diaz, D. Su, R.R. Adzic, E. Stach, J. Li, C.B. Murray, *ACS Nano* 6(2012), 2818-2825
10. V. Mazumder, S.H. Sun, *J. Am. Chem. Soc*. 131(2009) 4588-4589
11. Z.Y. Bai, L. Yang, L. Li, J. Lv, K. Wang, J. Zhan, *J. Phys. Chem*. C 113 (2009) 10568–10573.
12. B.H. Wu, D. Hu, J. Kuang, J. H. Chen, *Angew. Chem. Int. Ed*. 48 (2009) 4751-4754.
13. Y.G. Li, , W. Zhou, H.L. Wang, L.M. Xie, Y.Y. Liang, F. Wei, J.C. Idrobo, S.J. Pennycook, H.J. Dai, *Nature Nanotechnology* 7(2012) 394-400.
14. Y.J. Li, Y.J. Li, E.B. Zhu, T. McLouth, C.Y. Chiu, X.Q. Huang, Y. Huang, *J. Am. Chem. Soc*. 134 (2012)12326-12329.

15. B. Pierozynski, *Int. J. Electrochem. Sci*., 8 (2013) 634 - 642
16. M. Sevilla, G. Lota, A.B. Fuertes, *J. Power Sources* 171 (2007) 546-551.
17. Z.H Yan, M. Wang, B.X. Huang, R.M. Liu1, J.S. Zhao, *Int. J. Electrochem. Sci*., 8 (2013) 149 - 158
18. Z.Y. Bai, L. Yang, Y.M.Guo, C.G.Hu, *Chem. Commun*. 47(2011) 1752-1754.
19. T.R. Ohno, Y. Chen, S.E. Harvey, J.H. Weaver, R.E. Haufler, R.E. Smalley, *Phys. Rev*. B 44 (1991) 13747-13755.
20. G.H. Lee, J. H. Shim, H. Kang, K.M. Nam, H. Song, J.T. Park, *Chem. Commun*. 33 (2009) 5036-5038.
21. J.Z, Xu, S.Xu, J.Geng, G.X. Li, J.J. Zhu, *Ultrasonics Sonochemistry* 13(2006) 451-454.
22. N. Depalo, R. Comparelli, M. Striccoli, M.L. Curri, P. Fini, L. Giotta, A. Agostiano, *J. Phys. Chem. B* 110(2006) 17388-17399.
23. D. Iohara, F. Hirayama, K. Higashi, K. Yamamoto, K. Uekama, *Mol. Pharmaceutics* 8(2011) 1276–1284.
24. Z.Y. Bai, Y.M.Guo, L. Yang, L. Li, W.J. Li, P.L. Xu,C.G.Hu, *J Power Sources* 196 (2011): 6232-6237.
25. E.Y. Kim, Z.G. Gao, J.S. Park, H. Li, K. Han, *Int. J. Pharm.* 233 (2002) 159–167
26. C. Garnero, A. Zoppi, D. Genovese, M. Longhi, *Carbohydrate Research* 345(2010) 2550-2556.
27. M.J. Weaver, S.C. Chang, L.W.H. Leung, X. Jiang, M. Rubel, M. Szklarczyk, D. Zurawski, A. Wieckowski, *J. Electroanal. Chem* 327 (1992) 247-260.
28. Y.C. Zhao, X.L. Yang, J.N. Tian, F.Y. Wang, L. Zhan, *J. Power Sources* 195 (2010) 4634-4640.